Volume 3 | Number 1 | January 2016

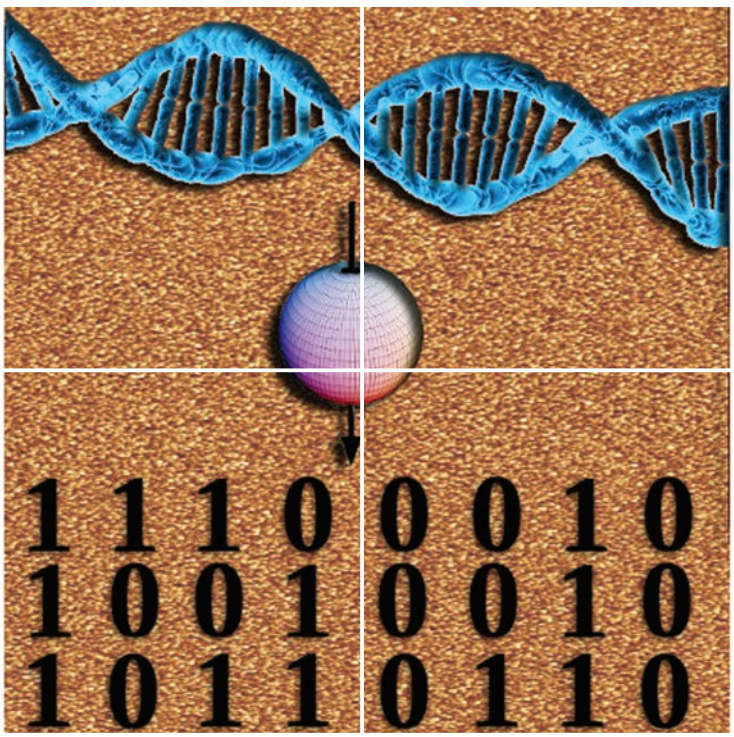

INORGANIC CHEMISTRY

FRONTIERS

Chinese Chemical Society
PEKING UNIVERSITY 1898
ROYAL SOCIETY OF CHEMISTRY

http://rsc.li/frontiers-inorganic

INORGANIC CHEMISTRY
FRONTIERS

REVIEW

Cite this: *Inorg. Chem. Front.*, 2016, **3**, 9

Solution synthesis protocols for shaping mixed valent oxide crystalline particles as robust catalytic materials

Jing-Wen Yu, Wei Zhu and Ya-Wen Zhang*

Received 26th September 2015,
Accepted 16th November 2015

DOI: 10.1039/c5qi00184f

rsc.li/frontiers-inorganic

Mixed valent oxides play a very important role in catalysis, as well as in gas sensing, biomedical engineering and electrochemistry. Because many chemical and physical processes occur on heterogeneous surfaces, the surface atomic structure becomes a critical factor affecting the properties of solid inorganic materials. Therefore, shape controlled synthesis, which can promise selective exposure of specific crystallographic planes with varied Miller indices for nano- and microcrystallites of metal oxides during the synthetic process, has turned into an important research topic in multidisciplinary fields. In this review, we summarize recent progress in the solution based shape controlled synthesis of several typical mixed valent oxide nano- and microcrystallites, including TiO_2, CeO_2, FeO_x, Cu_2O, CoO_x, MnO_x, WO_x, and MoO_3. The relationship between the surface structure of some mixed valent oxide nanomaterials and their chemical reactivity in heterogeneous catalysis and photocatalysis is also concisely discussed.

1. Introduction

Mixed valent oxides refer to oxides composed of cations with variable valency. They contain most of the transition metal oxides. Mixed valent oxides are not perfectly stoichiometric in most cases. Oxygen vacancies form to compensate for the imbalance of charge introduced by the reduced cation with the maintaining of crystal structure. It promotes not only the ion conductivity, but also the adsorption and dissociation of certain molecules (*e.g.*, O_2, *etc.*).[1,2] Mixed valent oxides possess oxygen storage and release properties by varying the valence.[3–6] These properties have made mixed valent oxides excellent solid state electrolytes and efficient catalysts and/or catalytic supports. The band gap of a significant portion of oxides falls into the range of semiconductors, such as 2.2 eV for Cu_2O, 2.3 eV for Fe_2O_3, 2.7 eV for WO_3, 3.2 eV for TiO_2, *etc.*[7] Therefore, mixed valent metal oxides can be also applied in photocatalysis and photovoltaic cells.[8,9] The magnetic and

Beijing National Laboratory for Molecular Sciences, State Key Laboratory of Rare Earth Materials Chemistry and Applications, PKU-HKU Joint Laboratory in Rare Earth Materials and Bioinorganic Chemistry, College of Chemistry and Molecular Engineering, Peking University, Beijing 100871, China. E-mail: ywzhang@pku.edu.cn; Fax: +86-10-62756787; Tel: +86-10-62756787

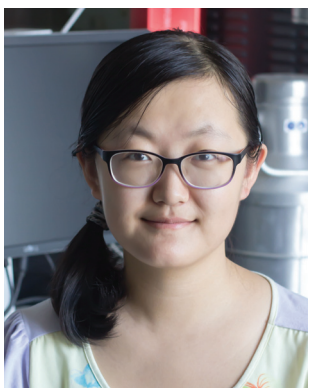

Jing-Wen Yu

Jing-wen Yu was born in April 1991 in Heilongjiang, China. She received her BSc degree in Chemistry from Peking University in 2013. Now she is working for her PhD degree under the supervision of Prof. Yawen Zhang at the College of Chemistry and Molecular Engineering, Peking University. Her current research focuses on the colloidal synthesis and catalytic property investigation of noble metal and metal oxide based nanocatalysts.

Wei Zhu

Wei Zhu received his BSc degree in Chemistry from Zhejiang University in 2009. He obtained his PhD degree at the College of Chemistry and Molecular Engineering, Peking University in 2014 under the supervision of Prof. Yawen Zhang. His research focuses on solution-based controllable syntheses of Pt-, Pd-, and Rh-based nanocrystals with well-defined morphologies and their structure-dependent catalytic properties toward typical model reactions.

electronic properties brought by the specific electron configurations of certain cations extend their applications in microelectronics and magnetism.[10,11] Furthermore, they can be applied in gas sensing and bio-diagnostic fields.[12,13]

Energy shortages and environmental protection are two challenging issues emerging with the burgeoning modern society. The application of highly efficient catalysts is one of the valid efficient methods to solve these two problems by promoting the atom economy of reactants and transforming waste into low- or non-harmful substances, and even useful resources.[14] In industrial processes, the most widely used catalysts are noble metals, in addition to exhaust treatments and fuel cells.[15–23] However, the catalysts have a high price and are sometimes easily poisoned.[24] It has been reported that low-cost mixed valent oxides with finely-modulated active structures can enhance their catalytic properties as supports or even replace the role of noble metal catalysts.[20–24] Mixed valent oxides exhibit increased catalytic properties not only in heterogeneous catalysis, but also in photocatalysis. In particular, metal oxide semiconductors such as TiO_2 have gained wide interest from researchers working in various disciplines.

As is known, shape-dependent catalytic properties are embodied in the modulation of active sites, and oxygen vacancies for mixed valent oxides, especially by exposing specific facets. Shape-control is one typical method that can be achieved *via* diverse wet chemistry routes, to unravel the intrinsic active sites during catalytic processes. It was found that there were many complicated aspects (*e.g.*, concentration of oxygen vacancies, ratio of highly-unsaturated-coordinated atoms, *etc.*) affecting the catalytic properties through the adjustment of the size of nanocatalysts.[25,26] However, control over the shape (*i.e.*, exposed facets) of the nanocrystals (NCs) could manipulate the arrangement of surface atoms. Adsorption sites, adsorption energy, and formation as well as mobility of oxygen vacancies might also be tuned on different crystal planes. Therefore, well-shaped oxide NCs can provide good models for the investigation of active structure-related catalytic properties. However, a surface reconstruction process may occur with catalytic processing at high temperatures. Also the composition of catalysts may change under an oxidative or reductive atmosphere.[27] *In situ* research on the changes of structure and composition are called for urgently, with the purpose of figuring out the realistic active sites.

Because mixed valent oxides are so important, many reviews relevant to their synthesis and applications in catalysis have already been published. Cheon *et al.*[28] and Hyeon *et al.*[29] have reviewed the nonhydrolytic colloidal routes and non-aqueous sol–gel routes for the shape-controlled synthesis of metal oxide NCs. Nguyen and Do[30] reviewed the general strategies for the surfactant-assisted synthesis of colloidal metal oxide and mixed metal oxide NCs. Xie *et al.*[31] focused on the high-energy-surface engineering of metal oxide micro- and nanocrystallites. The applications of metal oxides in catalysis and environmental protection have also been reviewed by Pan *et al.*,[32] Sarikaya *et al.*[33] and Kolmakov and Moskovits,[34] respectively. But among them, few have focused on the shape-controlled synthesis routes or disclosed the underlying shape-control principles behind various synthesis routes. Thus, a review which systematically introduces common shape-controlled synthesis routes and the synthesis principles of mixed valent oxides is still in great need.

This review is organized by first explaining the five most used wet chemistry based shape-controlled synthetic routes of common mixed valent oxide with real synthesis cases, in order to show the general principles of controlling the exposed facets of nano- and microcrystallites of these metal oxide materials, which is then followed by reviewing some examples of mixed valent oxide NCs that demonstrate shape correlated structure sensitivities in some important catalytic reactions, and ending with a vision of the challenges we face and the prospects of this field.

Ya-Wen Zhang

Ya-wen Zhang is full professor and principle investigator at the College of Chemistry and Molecular Engineering of Peking University. The research interests of his group are rational design, controllable synthesis, ordered assembly, catalytic properties and structure–function relationships of rare earth and noble metal nanostructures. He has published more than 100 papers in peer-reviewed scientific journals and was a winner of the National Science Fund for Distinguished Young Scholars in 2010. He obtained his BSc degree, MSc degree, and PhD degree from Peking University in 1988, 1994 and 1997, respectively, and did postdoctoral research in the State Key Laboratory of Rare Earth Materials Chemistry and Applications of Peking University during 1998–2000, and has been a visiting scholar at the Department of Chemistry of the University of California at Berkeley and Lawrence Berkeley National Laboratory during 2006–2008.

2. General shape-controlled synthetic routes for mixed valent oxides

Basic crystal planes are stable due to their relatively low surface energy, so synthesized NCs are usually enclosed by these planes. Generally, the more stable the plane is, the lower the activity is. This discipline can be applied in many cases, because high energy planes probably promote the adsorption and dissociation of reactants. There are many examples such as CeO_2,[35–37] Cu_2O,[38] Co_3O_4,[22] γ-Fe_2O_3,[39] *etc.* Hence, fabricating nanocatalysts enclosed by specific planes with a high density of active sites is an efficient way to enhance the catalytic activity. Moreover, product selectivity in some reactions is also concerned with the crystal face exposed.[40] Consequently,

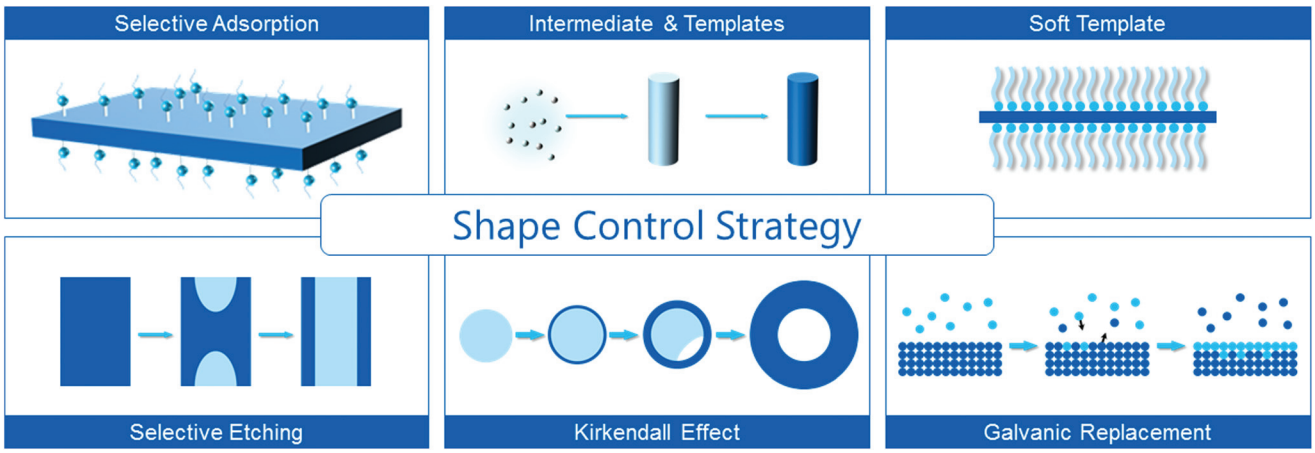

Scheme 1 General strategies used in the shape controlled synthesis of metal oxide NCs.

nanocrystallites with specific facets exposed are beneficial for acquiring enhanced product selectivity.

This section will focus on the main strategies for tuning certain crystallographic planes with variable active sites during the synthesis of mixed valent oxides, as illustrated in Scheme 1. Table 1 summarizes some of the mixed valent oxide nanocrystallites with well-defined shapes synthesized by these strategies.

2.1 Selective adsorption on specific crystal planes

Surface energy plays an important role in the energetics of nanoparticles (NPs). Besides the lattice strain which is drawn by grain boundaries, surface energy serves as the basic factor to control the thermodynamical equilibrium shape. The total free energy of the faceted particles can be expressed as:

$$G = \Sigma \gamma_i A_i$$

where γ_i represents the surface energy per unit area of a particular surface facet i, and A_i represents the surface area.[41] Hence, the free energy of a single crystalline particle is determined by the surface area and the surface energy per unit area. The Wulff construction is the minimum energy shape for a given volume. It is the most common geometry construction we can obtain in the synthesis.

In most cases, surfactants exist in solution-based syntheses. Surface adsorption can inhibit the accessibility of the monomers, thus retarding the linear growth rate of the particles. Unspecific surface adsorption of surfactants can indistinguishably reduce the surface energy to achieve size control on NCs. Sub-10 nm monodispersed oxide NCs can be easily acquired in the presence of surfactants (*e.g.*, oleic acid, *etc.*), otherwise only large NPs can be synthesized. Some functional groups, or ions (*i.e.*, shape inducing agents) exhibit specific surface adsorption capabilities towards different planes of metal oxides. They can reduce the surface energy of certain planes due to their variable coordination ability to different planes.

Under the presence of shape inducing agents, the other planes will vanish with the planes which have a strong interaction with the agents. For example, F^- can strongly adsorb on {001} planes of anatase TiO_2. Murray's group successfully synthesized a series of anatase TiO_2 NCs with various {001}/{101} ratios by tuning the precursors and cosurfactants to *in situ* release F^-.[42] Kim's group synthesized TiO_2 nanosheets with a {001} ratio of close to 60% using HF as a shape inducing agent. The average size of the {001} facets increased along with the amount of HF within 50–100 nm. The thickness showed an increasing trend in the range of 5–20 nm when using a lower concentration of HF.[43] Anatase single crystals with a large ratio of reactive facets were synthesized by a hydrothermal method with the addition of F^- as a morphology inducing agent by Yang and his co-workers (Fig. 1a).[44] Based on first-principles quantum chemical calculations, F^- terminated {001} is more energetically-favourable than {101} in classical Wulff constructions. With the combination of theoretical calculations and experiments, TiO_2 in micro-scale with up to 64% of {001} exposed facets was synthesized. Later on, anatase nanosheets with a high percentage (up to 89%) of {001} facets were synthesized *via* a hydrothermal method by taking the advantage of F^- as a shape inducing agent by Xie's group.[45] With the modification of reaction conditions, ultrathin nanosheets or nanosheets of several microns in length could be obtained. However, these nanosheets would grow into larger truncated bipyramidal single crystals through oriented attachment under hydrothermal conditions.[46] Hence, a structure reconstruction took place with rigorous conditions without the protection of F^-.

The selective adsorption of capped oleylamine ligands on {001} planes contributed to the anisotropic formation of MnO nanoplates. A nonhydrolytic sol–gel approach was achieved in the synthesis of MnO multipods by the oriented attachment and growth of truncated octahedral seeds.[47] Addition of selective adsorption agents was also a valid way of achieving the shape controlled synthesis of iron oxide NCs. Phosphate ions

Table 1 Summary of the examples of shape controllable syntheses of metal oxide NCs in this review

Nanostructures	Synthetic route	Key factors in the synthetic process	Synthetic cases
Cube	Selective adsorption	Cl^-, Br^- strongly bind on {100} facets	Magnetite[50]
	Selective adsorption	N-containing organic molecules strongly bind on {111} facets	Cu_2O[52–54]
	Selective adsorption	OA strongly binds on {200} facets	CeO_2 [58]
	Selective adsorption	Decanoic acid strongly binds on {001} facets	CeO_2 [59]
	pH	$NH_2OH{\cdot}HCl$	Cu_2O[71]
	pH	The base concentration (c_{NaOH})	CeO_2 [35]
Rod/tube/ring	Selective adsorption	PO_4^{3-} perpendicular to [001] axis	α-Fe_2O_3 [48,49]
	Selective etching	The selective proton-mediated etching	α-Fe_2O_3 [48]
	Intermediates	β-FeOOH precursor	α-Fe_2O_3 and γ-Fe_2O_3 [39]
	Intermediates	The production of $Ce(OH)_3$ nanotubes	CeO_2 [60,63]
	Intermediates	A rod-like acetate-containing cobalt hydroxide carbonate intermediate	Co_3O_4 [22]
	Surfactants	Trioctylphosphine different phosphines	MnO[70]
	pH	The base concentration (c_{NaOH})	CeO_2 [35]
Polyhedron	Selective adsorption	F^- strongly binds on {001} facets	TiO_2 [42,44]
	Selective adsorption	F^- strongly binds on {101} facets	α-Fe_2O_3 [51]
	Selective adsorption	N-containing organic molecules strongly bind on {111} facets	Cu_2O [52–54,56]
	pH	OH^- kinetics controlled	Cu_2O [38]
	pH	OH^-	Cu_2O [78]
	pH	$NH_2OH{\cdot}HCl$	Cu_2O [71]
	pH	The base concentration (c_{NaOH})	CeO_2 [35]
Sheet/belt	Selective adsorption	F^- strongly binds on {001} facets	TiO_2 [45,46]
	Intermediates	$Co(OH)_2$ nanosheets and $Co(CO_3)_{0.5}(OH)_{0.11}{\cdot}H_2O$ nanobelts	Co_3O_4 [61]
	Mineralizers	6-Aminohexanoic acid	CeO_2 [69]
	pH	Alkali-hydrothermal process	TiO_2 [75]
	pH	Alkali-hydrothermal process	TiO_2 [76]
	pH	Acid-hydrothermal process	TiO_2 [72]
Sphere	Mineralizers and surfactants	OA and 1-dodecanol	CoO [65]
Nanowire	Selective adsorption	N-containing organic molecules strongly bind on {111} facets	Cu_2O [55]
Other	Selective adsorption	OM strongly binds on {001} facets	MnO [47]
	Soft templates	OA, OM	TiO_2 [67]
	Soft templates	The aerosol-assisted self-assembly process	TiO_2 [68]
	Mineralizers and surfactants	Oleylamine and oleic acid stabilizers, sodium oleate or sodium diphosphate	CeO_2 [64]
	Mineralizers and surfactants	OA and 1-dodecanol	CoO[65]
	Surfactants	Oleylamine and trimethylamine-*N*-oxide	MnO[70]
	pH	Varying pH values	MnO[73]
	Galvanic replacement	Impregnating Mn_3O_4 nanocubes into iron(II) perchlorate solution	Mn_3O_4@Fe_2O_3 [82]
	Galvanic replacement		Cu_2O@CuO–Pd–Au[83]
	Selective etching	The geometric structure of templates	$Fe(OH)_x$ [79]
	Selective etching	Addition of ethanol leads to acidic etching of the {110} crystal faces on the nanocages	Cu_2O[80]
	Kirkendall effect		Fe_3O_4 [81]
	Kirkendall effect	Beam-irradiated	Co/CoO[84]
	Kirkendall effect	Beam-irradiated	Co/CoO[85]

were proposed to stabilize the planes along the [001] direction in hematite.[48,49] Associated with the coordinate-assisted dissolution process of PO_4^{3-}, hematite nanotubes formed *via* a spindle like intermediate under hydrothermal conditions with an appropriate pH value.[48] When the ratio of PO_4^{3-}/Fe^{3+} was adjusted in a moderate range, monodisperse hematite NCs with tunable aspect-ratio were synthesized *via* a programmed microwave-hydrothermal method by Yu's group.[49] PO_4^{3-} sup-

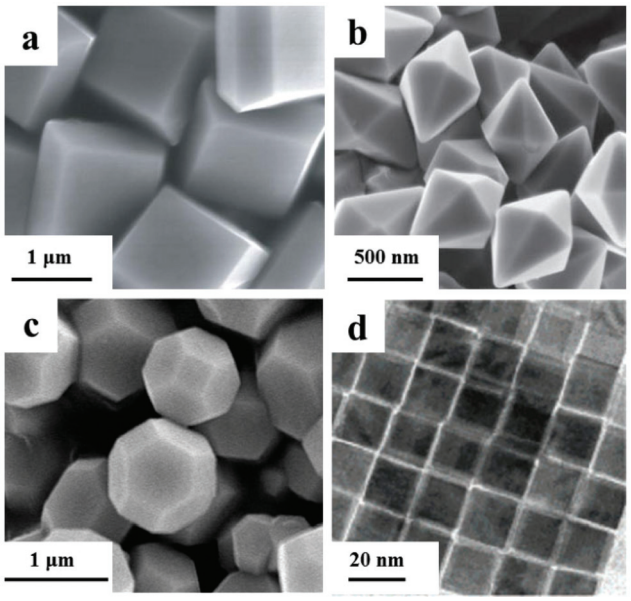

Fig. 1 Scanning electron microscopy (SEM) images of (a) TiO_2 polyhedrons (modified with permission from ref. 44, copyright 2008 Nature Publishing Group), (b) α-Fe_2O_3 dodecahedra (modified with permission from ref. 51, copyright 2010 Wiley-VCH), field-emission scanning electron microscopy (FESEM) image of (c) Cu_2O polyhedrons (modified with permission from ref. 53, copyright the Royal Society of Chemistry 2009), transmission electron microscopy (TEM) image of (d) ceria nanocubes (modified with permission from ref. 58, copyright 2006 American Chemical Society).

pressed the growth of planes perpendicular to the [001] axis; spindle-shaped NCs were favored to generate at a high PO_4^{3-}/Fe^{3+} ratio. Cl^- and Br^- were reported to be selective adsorbents on the {100} planes of magnetite. Magnetite nanocubes formed in the presence of Cl^- and Br^- during the thermolysis synthesis.[50] However, F^- tends to be selectively adsorbed on the {101} planes of hematite. Single crystalline α-Fe_2O_3 dodecahedral NCs enclosed by twelve {101} facets and octodecahedral NCs enclosed by twelve {101} facets and six {111} facets were synthesized *via* a F^--containing hydrothermal method (Fig. 1b and Scheme 2).[51] Halide ions and phosphate ions were revealed to have a selective adsorption effect in the shape controlled synthesis of iron oxide NCs. The arrangements of atom arrays on these low-index facets of iron oxides are different,

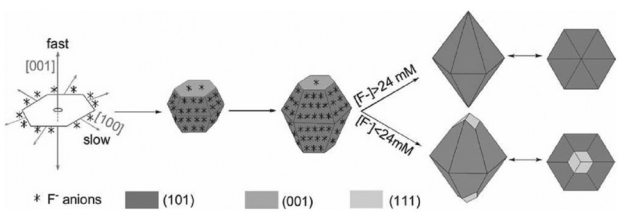

Scheme 2 Sketch of the growth mechanism of dodecahedral and octodecahedral α-Fe_2O_3 particles (modified with permission from ref. 51, copyright 2010 Wiley-VCH).

thus providing different coordination environments for various ions or functional groups.[50]

Compared with the {100} plane of Cu_2O, the {111} plane is a polar plane. The {111} plane can be terminated by a pure copper layer or an oxygen layer. Due to the strong coordination between Cu(I) and N, the {111} plane is adhered by some nitrogen-containing molecules. This "selective adsorption" strategy was applied to guide the design of the synthesis pathway and interpret the possible formation mechanism of Cu_2O NCs. Self-assembled sub-100 nm nanocubes and rhombic dodecahedra were acquired in almost 100% selectivity by Zeng's group.[52] *N*-Hexadecylamine was a generalist in this work: the chelating ligand, phase-transferring agent, reducing agent, shape inducing agent, and capping agent. Also Han and his co-workers have proved polyvinylpyrrolidone (PVP) to be a selective adsorption agent on the {111} planes of Cu_2O (Fig. 1c).[53] Nanocubes, truncated nanooctahedra, nanooctahedra, and star-shaped nanoparticles were obtained by varying the amount of PVP and reaction time.[54] In addition, N-containing organic molecules (*o*-anisidine, pyrrole, or 2,5-dimethoxyaniline) also acting as reducing agents were verified to be the key factor in controlling the 1D growth of Cu_2O nanowires.[55] Li and his co-workers suggested that the polymers *in situ* formed from the reducing agents selectively adsorbed on the planes of Cu_2O. The diameter and aspect ratio of the Cu_2O nanowires were tunable by varying the type/site of *ortho*-group of the reductants and temperature. Besides organic molecules, inorganic additives can also serve as shape inducing agents. With the introduction of inorganic cations and anions, Choi's group observed a distinct shape transformation of Cu_2O.[56] By the systematic comparison of additive ions, the conclusion was suggested as: NO_3^- stabilized {100} planes; NH_4^+ stabilized {110} planes; SO_4^{2-} stabilized {111} planes. Hence, the surface energy in the current situation decides whether the plane diminishes or expands.

Wang's group fabricated single-walled MoO_3 nanotubes with a thiol-assisted hydrothermal method.[57] Mo strongly interacted with sulphur-ending molecules. Due to the self-assembly of thiol, a MoO_3 single bilayer formed at the water–thiol interface. The MoO_3 bilayer rolled into single-walled nanotubes to release the strain which was caused by the unsaturated bonds from the edges.

Gao's group has developed a hydrothermal route to synthesize size controllable monodisperse ceria nanocubes by tuning the ratio of stabilizing agent/precursor (oleic acid (OLA)/Ce(III)) (Fig. 1d).[58] Because of the selective adsorption of OLA on {200} surfaces, small-sized CeO_2 nanocubes were formed by the fast growth of the {111} planes. Furthermore, supercritical solvent contributed a lot to the synthesis of monodisperse NCs, especially for the homogeneous reaction system with high temperature. Selective adsorption of decanoic acid on CeO_2 {001} facets can contribute to the formation of diverse Wulff constructions of CeO_2 NCs by tuning the total surface energy. It was proposed that large-sized nanocubes could be acquired through an oriented aggregation mediated precursor growth. Monodisperse sub-10 nm CeO_2 nanocubes

and truncated nanooctahedra were also synthesized by Adschiri and his co-workers *via* a supercritical hydrothermal method.[59]

2.2 Intermediate transformation

During the formation of oxides NCs, the final morphology of the NCs can inherit the shape of the intermediates (*e.g.*, hydroxides, metal basic carbonate, *etc.*). So by starting with different precursors which contain valent variable cations, we can obtain the final products with different shapes (Fig. 2).[60]

Co_3O_4 nanorods were considered hard to obtain through the direct isotropic growth of cubic Co_3O_4. A rod-like acetate-containing cobalt hydroxide carbonate intermediate is necessary for the anisotropic growth of Co_3O_4 nanorods. From the as-obtained NCs, the identically shaped NCs with other valences generally can be achieved by a mild redox post-treatment process.[22] Three types of Co_3O_4 nanostructures were synthesized through the precipitation under solvothermal conditions by Li's group.[61] The precursor of the Co_3O_4 nanosheets is the β-$Co(OH)_2$ nanosheets. And the precursor of the Co_3O_4 nanobelts is $Co(CO_3)_{0.5}(OH)_{0.11}{\cdot}H_2O$ nanobelts. These spinel NCs were with different exposed facets: nanosheets were primarily enclosed by {112} facets; nanocubes were enclosed by {001} facets; nanobelts were dominantly enclosed by {011} facets.

In the synthesis of CeO_2 NCs, $Ce(OH)_3$ with a hexagonal phase is proposed to be the intermediate which contains Ce(III). Nanorods and nanotubes can be obtained from the trivalent precursor, whereas only polyhedra were synthesized from the tetravalent precursor.[35,60] Combined with the control of reaction rate and the use of Ce(III) precursors, the template-free synthesis of 1D CeO_2 nanostructures has been reported by many groups. Except for the templated synthesis,[62] unstable hexagonal $Ce(OH)_3$ intermediates were proposed to be the key for anisotropic growth of the 1D NCs. A hydrothermal approach was applied to synthesize CeO_2 nanorods with {110} and {001} facets exposed by Li and his coworkers.[63] Starting with a Ce(III) salt as a precursor, $Ce(OH)_3$ intermediates formed after the direct hydrolysis of Ce^{3+}. The hexagonal intermediates tended to grow along its *c* axis, because the (001) facets were unstable. Uniform CeO_2 nanorods finally formed after the oxidation of metastable $Ce(OH)_3$ intermediates. Meanwhile, Tang and his colleagues have fabricated CeO_2 nanotubes through a similar hydrothermal method without oxygen and substitution of $Ce(NO_3)_3$ with $CeCl_3$.[60] Hence, unstable $Ce(OH)_3$ nanotubes could form during the synthesis. After the thermal post-treatment of the obtained $Ce(OH)_3$ nanotubes with Ar and NH_3, a smooth structure modification took place from $Ce(OH)_3$ to CeO_2 nanotubes. Most CeO_2 nanotubes grew along the [110] orientation.

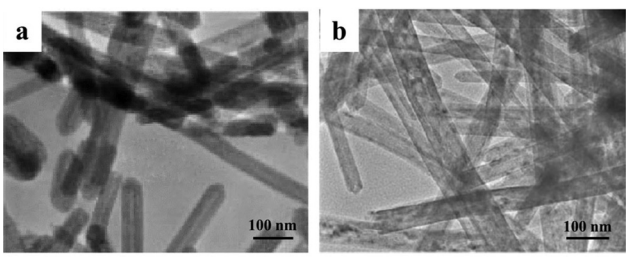

Fig. 2 TEM images of (a) $Ce(OH)_3$ nanotubes synthesized at 120 °C, (b) CeO_2 nanotubes formed during controlled annealing of the $Ce(OH)_3$ nanotubes synthesized at 120 °C (modified with permission from ref. 60, copyright 2005 Wiley-VCH).

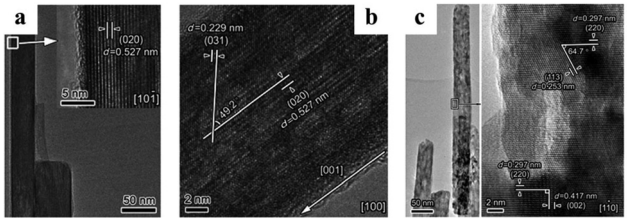

Fig. 3 (a) Low-magnification TEM image of a single β-FeOOH nanorod viewed along the [10$\bar{1}$] direction. The insert HRTEM image indicates that the nanorod exposes the {010} planes. (b) Another HRTEM image viewed along the [100] orientation, also showing the preferential exposure of the {010} planes, (c) low- and high-magnification TEM images of a single g-Fe_2O_3 nanorod, indicating the dominant exposure of the {110} and {001} planes (modified with permission from ref. 39, copyright 2012 Wiley-VCH).

1D iron oxide NCs were fabricated through the intermediate method. Shen's group synthesized α-Fe_2O_3 and γ-Fe_2O_3 nanorods dominantly enclosed by {110} and {001} facets by the precipitation reaction of $FeCl_3$ in poly(ethyleneglycol) (PEG) (Fig. 3).[39] A rod-like β-FeOOH precursor was first obtained in the hydrolysis. γ-Fe_2O_3 nanorods finally formed by aging the β-FeOOH precursor. Meanwhile, α-Fe_2O_3 nanorods were generated by calcination. Two phases of Fe_2O_3 NCs inherited the morphology from the same intermediate.

2.3 Surfactants as mineralizers and soft templates

Surfactants are widely used in the synthesis of NCs because of their capability of amphipathy. They can be adsorbed on the surface of NCs and regulate the surface energy. Thus, surfactants can be employed as stabilizers,[64] capping agents,[65,66] activating reagents,[65] inhibiting reagents,[65] selective adsorbents,[66] structure directing agents,[67] and when forming complex constructions, used as soft templates.[67,68]

Sometimes surfactants are employed as oxidants[66] for their oxidizing ability, or mineralizers[64] for their ability to promote the crystallization process of NPs with altered shapes. Therefore, surfactants play an important role in the size and morphology control of mixed valent metal oxides.

Unlike the readily-obtained 1D CeO_2 nanostructures, there are only a few reports of the well-controlled synthesis of 2D CeO_2 NCs. It is difficult to retard the growth along the *c* axis of hexagonal $Ce(OH)_3$ intermediates and boost the growth on *a*–*b* planes. However, the assembly and coalescence of small NPs or the formation of organic–inorganic complexes can result in the formation of 2D CeO_2 NCs. Single crystalline CeO_2 nanosheets were prepared through the slow, continuous addition of Ce(III) precursors into 6-aminohexanoic acid solu-

tion by Xia's group.[69] The ultra-thin nanosheets had a thickness of 2.2 nm and were up to 4 μm in width. A slow assembly and growth mechanism was proposed. Time sequence reactions revealed that small NPs formed when the reaction was initiated. These particles assembled and grew into polycrystalline nanosheets. With prolonged time, the intermediates reorientated and formed the final products. Murray and his colleagues reported the synthetic route of CeO_2 nanoplates enclosed by six {111} planes by the thermal decomposition of cerium acetate hydrate in oleylamine and oleic acid (Fig. 4a).[64] Sodium oleate or sodium diphosphate served as mineralizers in the reaction. The plates were about 2 nm in thickness. The size and shape of the plates were tuneable by changing the reaction parameters. Square ceria nanoplates were synthesized with sodium diphosphate as the mineralizer while the mineralizer for forming elongated ceria nanoplates was sodium oleate. The reason why mineralizers with different anions can affect the nanostructures of mixed valent oxides is still unclear. Nonetheless, the addition of mineralizer is crucial to control the shape or size of metal oxides NCs in many cases probably due to the disturbance toward the nucleation stage. It can not only increase the yield of mixed valent oxide NCs, but also promote their crystallization process.

A thermolysis route was an adept way to synthesise cobalt oxide NCs with small sizes. It managed the preparation of tetrahedron-, sphere-, polypod-, and flower-shaped NCs through control of the nucleation and growth stage (Fig. 4b).[65] The crystalline phase of cobalt oxide nuclei strongly influenced the final shapes. OA retarded the formation of CoO NCs, whereas 1-dodecanol activated the reaction. By the adjustment of the ratio of OA to 1-dodecanol, the reaction rate could be finely tuned. The faster the reaction rate was, the more complex the final morphology was. 5–40 nm MnO NPs and (7–10 nm) × (30–140 nm) MnO nanorods were obtained by the decomposition of $Mn_2(CO)_{10}$ in trioctylphosphine.[70] The diameters and lengths of the nanorods were varied by using different species of phosphines. The cooperative interaction from oleylamine and trioctylphosphine resulted in the rod morphology. The two kinds of surfactants with different stabilizing capabilities were used under kinetically controlled conditions, and contributed to form MnO nanorods. (10.2 ± 0.6) nm × (6.8 ± 0.4) nm MnO nanoplates enclosed by {100} and {110} planes were synthesized by the thermolysis of $Mn(ac)_2$ (ac = acetic acid) in oleylamine. (12.2 ± 0.6) nm × (5.6 ± 0.3) Mn_3O_4 nanoplates enclosed by {001} planes were obtained by the oxidation of MnO nanoplates (Fig. 4c).[66]

Self-assembled surfactants can be regarded as a kind of soft template. Metal–organic intermediates are usually proposed to be formed at the initial stage of growth of NCs. The organic–inorganic complex tends to self-assemble on the interface due to the hydrophobic effect. Under the confinement of the self-assembled template, oxide NCs could evolve into different types of structures, *i.e.* micelles, cylinders, planar structures, *etc*. The strategy is applied in the synthesis and fabrication of self-organized ultrathin oxide NCs for many transition metal oxides and rare earth oxides.[67] For example, the soft template method can be applied to synthesize ultra-thin TiO_2 nanostructures. Yang's group fabricated ultrathin (sub-2 nm, down to one-unit cell) anatase nanorods *via* the thermodecomposition of titanium isopropoxide in oleic acid and oleylamine (Fig. 4d and Scheme 3).[67]

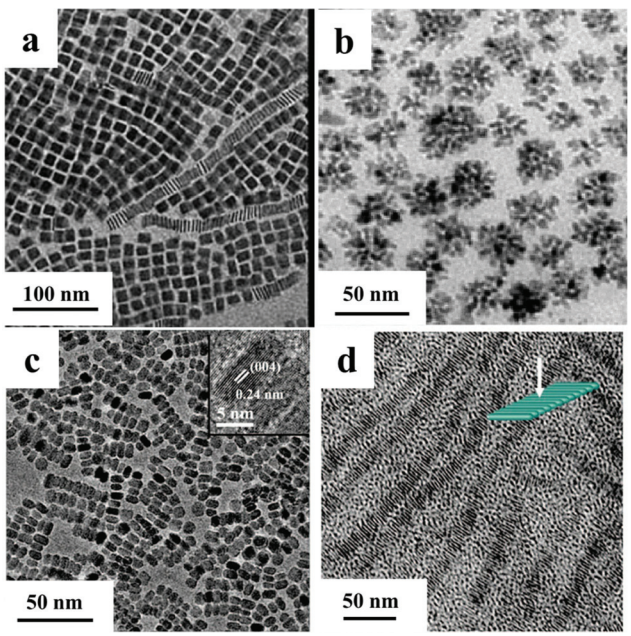

Fig. 4 TEM images of (a) square ceria nanoplates (modified with permission from ref. 64, copyright 2011 Wiley-VCH), (b) CoO nanostructures (modified with permission from ref. 65, copyright 2008 American Chemical Society), (c) farfetched "face-to-face" self-assembly nanoarrays and HRTEM (inset) images of Mn_3O_4 nanoplates (modified with permission from ref. 66, copyright 2009 American Chemical Society), (d) the as-prepared TiO_2 NRs and their superstructures (modified with the permission from ref. 67, copyright 2009 American Chemical Society).

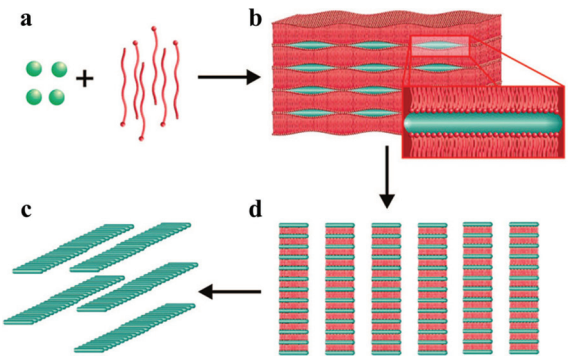

Scheme 3 Schematic illustration for the synthesis of ultrathin nanostructures and their assembly. (a) The inorganic precursor species were mixed with surfactants, then the mixture formed metal–surfactant complex monomers. (b) The complex monomers and excess surfactants were organized into layered mesostructures. (c) After the reaction, crystalline nanorods evolved from the layered mesostructures. (d) The layered mesostructures were then disrupted, and the nanorods self-assembled into 1D superstructures. (modified with permission from ref. 67, copyright 2009 American Chemical Society).

First, titanium isopropoxide or titanium butoxide was mixed with octadecene and oleic acid (Scheme 3a), then the mixture formed metal–surfactant complex monomers. These complex monomers and remaining surfactants were organized into layered mesostructures (Scheme 3b) which contained many nanoscale reactive pockets for oxide NCs to nucleate and grow. The inorganic portion of the monomers was largely restricted in the hydrophilic reactive pockets, and the metal–surfactant complexes were decomposed *in situ* at high temperature to produce a metal–oxygen network through an ester elimination process. After the reaction was heated at a given temperature for several hours, crystalline nanorods evolved from the layered mesostructures. The layered mesostructures were then disrupted, and the nanorods spontaneously self-assembled into 1D superstructures (Scheme 3c and d). Also diverse mesoporous metal oxide nanostructures can be produced *via* the soft template method developed by Stucky's group.[68]

2.4 pH value adjustment

Surfactants are commonly applied during the formation of oxide NCs, but some of them will be adsorbed at the active sites of oxide NCs and thus impede the catalytic properties of the nanomaterials. Currently, a synthetic strategy without using surfactants has become one of the hotspots of nanocrystalline synthesis. The regulation of acid–base balance (namely the pH value of the synthesis solution) is widely applied in these studies. Regulation of acid–base can adjust the shapes of mixed valent oxide NCs as a result of the interplay between thermodynamics and kinetics.

Acid–base balance can affect a lot of key factors in synthetic process, for example, hydrion concentration, which can adjust the hydrolysis rate of metal oxide precursor and afterwards can regulate the dissolution/recrystallization process,[35] and the growth rate of metal oxide NCs.[71] It can also control the shape of intermediates, whose morphology will be inherited by the mixed valent oxide.[35,72,73] Acid–base balance can certainly modulate the pH of the solution, which leads to different stabilities of metal oxide and metal hydroxide. Surface charge and surface potential of mixed valent oxides, which can affect the synthesis of specific facets, can also be adjusted by changing the acid–base balance.

The pH value plays a vital role in the hydrothermal synthesis. The hydrothermal method can always be divided into two routes, *i.e.*, the alkali-hydrothermal process and the acid-hydrothermal process. The precursor is always hydrolysed in alkali or acid solution to form the mixed valent oxide. So the pH value of the solution is very important in the hydrolyzation of the precursor.

The synthesis of TiO_2 nanobelts is an appropriate example. When dispersed in water, the reactions that take place are related to the pH value of the solution, as eqn (1)–(3) show:[74]

$$3TiO_2 + 2NaOH \rightarrow Na_2Ti_3O_7 + H_2O \quad (1)$$

$$Na_2Ti_3O_7 + 2HCl \rightarrow H_2Ti_3O_7 + 2NaCl \quad (2)$$

$$H_2Ti_3O_7 \rightarrow 3TiO_2 + H_2O \quad (3)$$

The anatase phase TiO_2 belt with the growth direction of [010] can be obtained from an alkali-hydrothermal process (Fig. 5a).[75] By carefully keeping the reactants uniform, anatase TiO_2 nanobelts with dominant {100} facets can also be prepared by an alkali-hydrothermal process.[76] During the acid-hydrothermal process, by delicate control of the rate of hydrolysis of the titanium precursor under acid conditions, rutile TiO_2 nanobelts with the [001] growth direction can be formed.[72] Zhao and his co-workers systematically investigated the phase transition of different crystalline phases of TiO_2, which were synthesized in different concentrations of NaOH or HCl, followed by calcining at 400, 600, 800 or 1000 °C.[77] Under high acidity condition, it was beneficial to form rutile TiO_2 nanorods. When pH values were close to neutral, it was favourable to form anatase TiO_2 NCs. In a mainly NaOH solution, which had a pH value of about 13, brookite TiO_2 nanoflowers were easily formed. Then, with increasing NaOH concentration, the product was sodium titanate.

Polyhedral 50-facet Cu_2O microcrystals were prepared by primarily controlling the concentration of OH^- and the volume ratio of ethanol to water by Wang and his co-workers (Fig. 5b).[38] From the geometry model, it was deduced that the microcrystals were bound with 24 high-index {311} facets. This can probably be ascribed to the existence of a high percentage of high index facets. Similar 50-facet Cu_2O microcrystals were synthesized by a facile seed-mediated method.[78] The difference

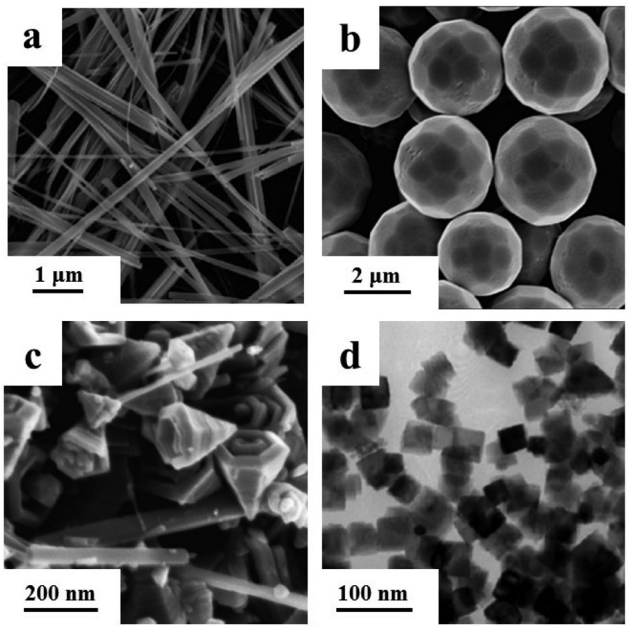

Fig. 5 (a) SEM image of anatase TiO_2 nanobelts (modified with permission from ref. 75, copyright 2010 American Chemical Society); (b) FESEM image of polyhedral 50-facet Cu_2O microcrystals (modified with permission from ref. 38, copyright 2010 American Chemical Society); (c) FESEM image of manganite γ-MnOOH/γ-MnO_2 (modified with permission from ref. 73, copyright the Royal Society of Chemistry 2009); (d) TEM image of CeO_2 nanocubes (modified with permission from ref. 35, copyright 2005 American Chemical Society).

was that the obtained structure was bound with 24 high-index {211} facets, and 8 low-index {111} facets, 6 low-index {100} facets and 12 low-index {110} facets. Recently, Huang and his co-workers reported a series of shape transformations of Cu_2O NCs could be adjusted from nanocubes enclosed with {100} planes to rhombic dodecahedra enclosed with {110} planes by the simple manipulation of the addition of $NH_2OH{\cdot}HCl$.[71]

It is facile to obtain high quality manganese oxide nanostructures through a low-temperature liquid-phase comproportionation. Manganite γ-MnOOH/groutite α-MnOOH mixed nanorods, and γ-MnO_2 nanocones were acquired by the reaction between MnO_4^- and Mn^{2+} with varying pH values at 368 K (Fig. 5c).[73] With different initial pH values and different media, Mn^{2+} and MnO_4^- were in different steady states and followed different reaction pathways. So, different intermediates, such as α-MnOOH nanorods and birnessite δ-MnO_2 sheets were formed, and then different MO_x nanostructures were obtained.

Zhang and Yan's group found that CeO_2 nanopolyhedra, nanorods, and nanocubes could be selectively formed by adjusting the base concentration (c_{NaOH}) and hydrothermal temperature, using $Ce(NO_3)_3$ as the cerium source (Fig. 5d).[35] Changing the base concentration can also prepare CeO_2 nanotubes, by using $CeCl_3$ as the cerium source.[60]

2.5 Selective etching, galvanic replacement and the Kirkendall effect

Selective etching, galvanic replacement and the Kirkendall effect are used in the production of hollow inorganic structures, such as nanotubes, nanoframes and nanocages. High energy facets usually appear at the transition of low energy facets. Hollow structures surely have more such transitions, which result in the formation of more high energy facets.

In the synthesis of Fe_2O_3 nanotubes, a hollow structure was achieved by the selective proton-mediated etching of Fe_2O_3 nanorods.[48] With the protection of the phosphate group on the walls of the nanorods, proton etching only took place at the two ends. Nanotubes were finally formed through this approach. Furthermore, several hollow iron oxide structures were reported by the selective etching method. Those frameworks could be engineered by the geometry structures of templates. Differently shaped hollow structures, even double-walled, could be obtained *via* the growth and etching approach of Lou's group.[79]

Cu_2O nanoframes with only {110} skeleton facets and with only {100} skeleton facets were synthesized by one continuous reaction leading to a preferential growth and etching process (Fig. 6a and Scheme 4).[80]

Galvanic exchange (also known as transmetalation) is another generally applicable and promising method for creating designed NPs with hollow structures, thereby altering their physical properties (Scheme 1). Galvanic exchange is a common way to synthesize bimetallic NPs.[81] Recently, it was proved also appropriate for the synthesis of mixed valent oxide hollow structures.[82]

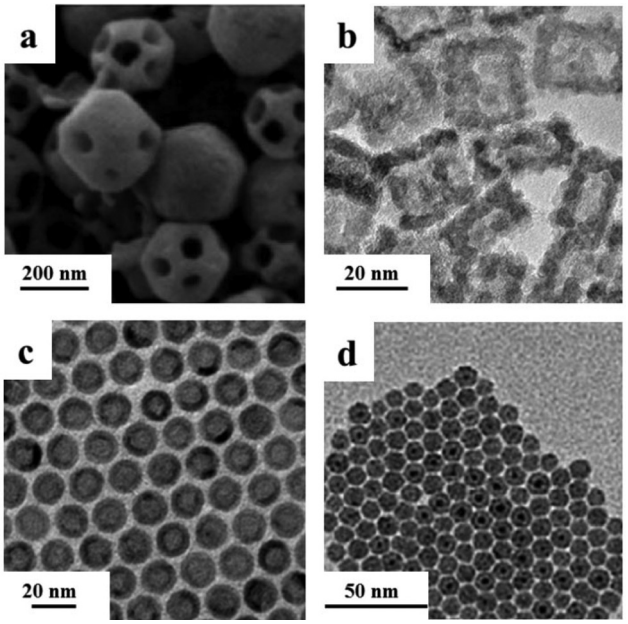

Fig. 6 (a) SEM image of the truncated rhombic dodecahedral Cu_2O nanoframes (modified with permission from ref. 80, copyright 2008 American Chemical Society); TEM images of (b) γ-Fe_2O_3 nanocages (modified with permission from ref. 82, copyright 2013 by the American Association for the Advancement of Science); (c) hollow Fe_3O_4 nanoparticles (modified with permission from ref. 84, copyright 2007 Wiley-VCH) and (d) Co nanoparticles after oxidation (modified with permission from ref. 85, copyright 2013 American Chemical Society).

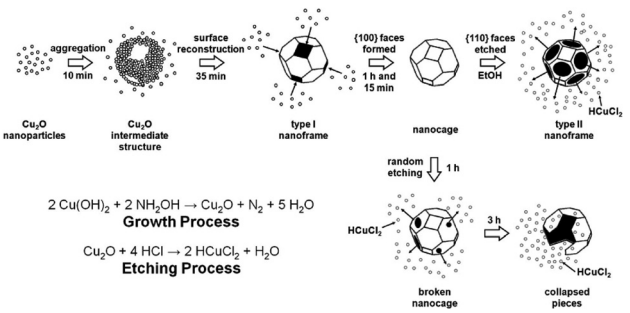

Scheme 4 Schematic illustration of the growth and etching mechanisms in the synthesis of Cu_2O nanoframes and nanocages (modified with the permission from ref. 80, copyright 2008 American Chemical Society).

Galvanic exchange is driven by the difference between the reduction potentials of the two materials. The general stages of galvanic exchange are described as follows: first, a nanostructure of the less noble material is synthesized. Then, a solution containing cations of a more noble material which has a lower reduction potential is added. After the addition of the noble material, some portion of the NPs of the less noble material, which serves as a sacrificial template, is oxidized and transferred into solution, while the more noble metal is reduced and deposited. The structure and composition of the

products are continuously affected by the interaction between the more and less noble materials, as galvanic exchange reactions proceed. Initially, alloy shells usually grow on the less noble material NPs. During the galvanic exchange procedure, dealloying may also occur, with the less noble material being removed from the composite. Alloying and dealloying drive morphological change into hollow nanostructures, normally. The final stage of dealloying can lead to the breakup of the nanostructure. So, galvanic exchange reactions are often stopped before completion to synthesise hollow structures.[81]

Hyeon's group reported a general galvanic replacement method for the synthesis of metal oxide nanoboxes or nanocages (Fig. 6b and Scheme 5).[82] A galvanic replacement reaction took place by impregnating Mn_3O_4 nanocubes into iron(II) perchlorate solution. Mn(III) dissolved into solution with the oxidative precipitation of Fe(II). With the increase of the concentration of Fe(II), the shape evolved from Mn_3O_4/γ-Fe_2O_3 nanoboxes to γ-Fe_2O_3 nanocages. This redox etching approach can be extended to Co_3O_4/SnO_2 and Mn_3O_4/SnO_2 systems.

Li and Lang's group reported that a hollow Cu_2O@CuO/(Au–Pd) heterostructure can be formed by the galvanic replacement reaction of Cu_2O cubes, which acted as a sacrificial template, with bimetallic precursors in an EtOH solution at room temperature. The surface of the Cu_2O nanocubes were oxidized into CuO, forming hollow Cu_2O–CuO core–shell structures, while Pd^{2+} and Au^{3+} were reduced to Pd(0) and Au(0). Then Au–Pd alloy NPs were deposited on the hollow Cu_2O–CuO core–shell structure.[83]

The Kirkendall effect is also an efficient way to create nanocrystallites with a hollow structure. In core–shell structures, when the species from the core of the NPs diffuse outward faster than the inward diffusion of the reactive species, a void forms inside the NPs. The void formed through the unequal diffusion is a result of the Kirkendall effect (Scheme 1). The Kirkendall effect has got significant attention due to its potential for synthesizing uniquely tailored compositions and nanostructures.[81]

For example, by the oxidation of up-layers on iron NPs, monodisperse hollow spheres were prepared by the controlled oxidation of Fe–Fe_3O_4 nanoparticles (Fig. 6c and Scheme 6).[84] The Fe nanoparticles synthesized from the thermal decomposition of [$Fe(CO)_5$] were not chemically stable, and were easily oxidized. When exposed to air, core–shell Fe–Fe_3O_4 structures were in the amorphous state, with both Fe and Fe_3O_4. Controlled oxidation of these core–shell nanoparticles led to the formation of intermediate core–shell–void Fe–Fe_3O_4, and further to hollow Fe_3O_4 nanoparticles that contained polycrystalline Fe_3O_4 grains.

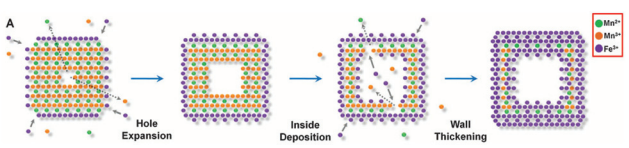

Scheme 5 Schematic illustration of the transformation of Mn_3O_4 NCs, showing the evolution of their morphology *via* the localized dissolution of Mn_3O_4 and the surface precipitation of γ-Fe_2O_3 (modified with permission from ref. 82, copyright 2013 by the American Association for the Advancement of Science).

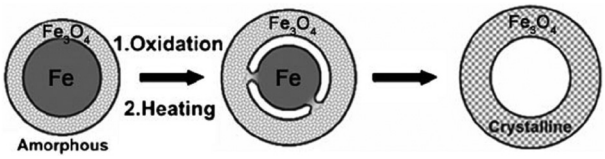

Scheme 6 Synthesis of core–shell–void Fe–Fe_3O_4 and hollow Fe_3O_4 nanoparticles from Fe–Fe_3O_4 nanoparticle seeds (modified with permission from ref. 84, copyright 2007 Wiley-VCH).

Pileni's group reported an electron beam-irradiation method to synthesize a CoO hollow structure. It demonstrated that the electron beam could also play an important role in the nanoscale Kirkendall effect (Fig. 6d).[85] Their subsequent article demonstrated that the 2D ordering and crystallinity of Co nanoparticles controlled the diffusion process of oxygen.[86]

3. Structure–reactivity relationship of mixed valent oxides in catalysis

Mixed valent oxides exhibit promoted catalytic properties not only in heterogeneous catalysis, but also in photocatalysis and photovoltaic devices. Both the adsorption energy of small molecules and the bandgap can be adjusted by different exposed facets of the oxides. Structure-dependent catalytic properties of mixed valent oxides were investigated based on these well-shaped nanostructures.

Mixed valent oxides are widely used as catalysts or supports in O_2-related heterogeneous reactions. Abundant oxygen vacancies generated by the non-stoichiometric composition endue oxides with oxygen storage capability and promote the dissociation of oxygen molecules.[3–6] Meanwhile, mixed valent oxides can enhance catalytic activity as supports through a bifunctional effect or charging of metal catalysts.[20,87] The performance of mixed valent oxide photocatalysts can also be improved with similar research strategies.[44,45] However, their shape-dependent properties are roughly ascribed to the chemical activity of exposed facets. So a detailed intrinsic photocatalytic mechanism is still in demand.

In this section, we will show some examples in shape-controlled mixed valent oxides as catalysts and supports in heterogeneous catalysis and photocatalysis. Furthermore, we will discuss their structure-dependent catalytic properties in some catalytic processes.

3.1 Shape-controlled mixed valent oxides as heterogeneous catalysts

Although the active sites might be different in various catalytic oxygen-related reactions, oxygen vacancies (*i.e.*, one of the

defect sites in oxides) have been generally considered as the active sites in these reactions catalysed by mixed valent oxides.

For CO oxidation which has been used as a benchmark reaction to evaluate the activity of catalysts, oxygen vacancies promoted the adsorption and dissociation of oxygen molecules and accelerated the reaction. According to the conclusions drawn from STM and DFT calculations, surface and subsurface oxygen vacancies are confined by the electron localization.[88] Hence, "defect engineering" is possible, by varying the ratio of cations with different valences or introducing foreign ions. Shape-selective synthesis is a convenient method of synthesising materials with easily formed oxygen vacancies on certain facets.

It was reported that defective CeO_2 NCs could be acquired with post-treatment under vacuum.[36] CO oxidation catalytic properties can be improved with the increase of defect sites (Fig. 7a). {100} and {110} planes of CeO_2 showed higher CO oxidation activity and oxygen storage capability than low energy {111} planes.[35] This result suggested that high OSC materials could be designed and obtained by a shape control synthetic strategy. Sayle *et al.* predicated that the ready formation of oxygen vacancies on (110) and (310) surfaces resulted in higher reactivity in the oxidation of CO than that of the (111) surface.[89] Conesa indicated that the required energy to form oxygen vacancies on (110) and (100) surfaces was less than that on the (111) surface.[90] The activity of CO oxidation for α-Fe_2O_3 follows the order {012} > {113} > {001}. The amount of chemisorbed CO followed the order below: pseudocube-Fe_2O_3-{012} NCs > bipyramid-Fe_2O_3-{113} NCs > plate-Fe_2O_3-{001}/{012} NCs. CO chemisorption could quantitatively reflect the amount of active sites on the surface of blank NCs. So, the catalytic activity in CO oxidation also followed the order below: pseudocube-Fe_2O_3-{012} NCs > bipyramid-Fe_2O_3-{113} NCs > plate-Fe_2O_3-{001}/{012} NCs.[91]

Furthermore, it was unravelled that the type of oxygen vacancies might contribute in varying degrees to the activity enhancement. In the case of CeO_2 nanorods, the oxygen vacancy clusters in large size were the dominant sites to enhance CO oxidation activity (Fig. 7b).[92] Doping lanthanides (Ln) into CeO_2 is also a robust approach to tune the formation of oxygen vacancies. The CO oxidation reactivity over CeO_2:Ln nanowires was dependent on the Ln dopants, and the turnover rates reached a maximum for the Nd-doped samples.[93] The doping of Gd^{3+} into CeO_2 also modulated the oxygen vacancies. This article promoted the anti-oxidation performance by doping Gd^{3+} into CeO_2 due to the modulation of the oxygen vacancies, and revealed that the anti-oxidation mechanism was associated with the state of the oxygen vacancies.[94] Hence, the assumption of "defect engineering" has been realized with simple chemical treatment, shape-selective synthesis, and a doping process. Identification and fabrication of efficient oxygen vacancy clusters could be a challenging task in defect engineering.

High index facets contain a high percentage of highly-unsaturated-coordinated atoms; they are proposed to exhibit superior catalytic activity. With the introduction of high index facets (*i.e.*, {311} facets), Cu_2O microcrystals showed higher CO oxidation activity than the structures bound with the three basic facets (Fig. 8a).[38] Hence, this is one acceptable route to design efficient catalysts by creating high index facets on the nanocatalysts. The order of adsorption energy on different planes varies with the species of adsorbates and substrates.

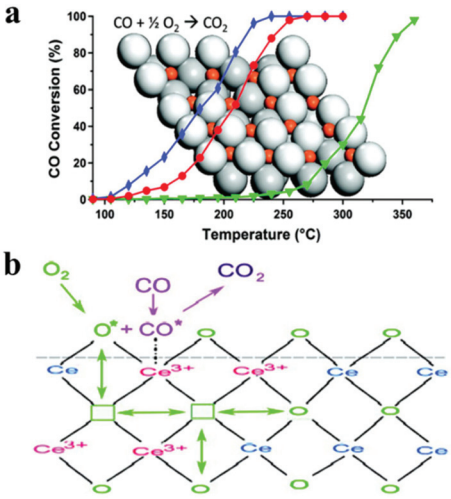

Fig. 7 (a) CO oxidation activity of CeO_2 NCs post-treated under ambient pressure or vacuum (the blue line presents the activity of nanorods treated under vacuum; the red line presents the activity of nanoparticles treated under vacuum, and the green line presents the activity of nanorods treated under ambient pressure) (modified with permission from ref. 36, copyright 2011 American Chemical Society); (b) scheme of the CO oxidation reaction catalysed by larger CeO_2 oxygen vacancy clusters (modified with permission from ref. 92, copyright 2009 American Chemical Society).

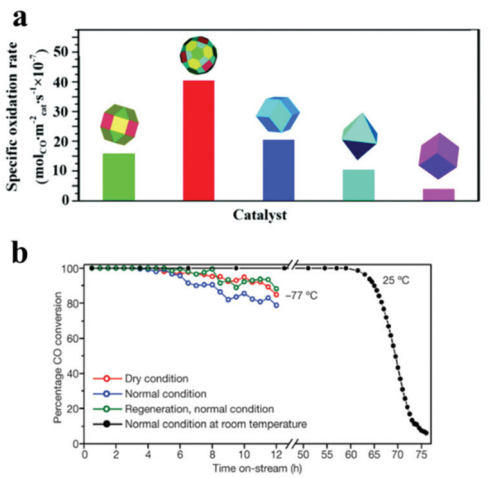

Fig. 8 (a) Specific oxidation rates of the CO oxidation reaction on various shaped Cu_2O microcrystals (modified with permission from ref. 38, copyright 2010 American Chemical Society); (b) CO oxidation stability test of Co_3O_4 nanorods under stream under different conditions (modified with permission from ref. 22, copyright 2009 Nature Publishing Group).

Therefore, the composition and arrangement of ions on the exposed surface determines the activity. Co^{3+} sites existing on the {110} planes of Co_3O_4 nanorods acted as the active sites for the oxidation of CO (Fig. 8b).[22] So the Co_3O_4 nanorods exhibited excellent activity and stability towards CO oxidation reactions at low temperatures. The hydrogenation of carbonyl sulfide (COS) was investigated over catalysts derived from nanocrystalline Co_3O_4 nanorods and nanopolyhedra. Compared with the Co_3O_4 nanopolyhedra, Co_3O_4 nanorods showed a higher activity in the presulfurization process and resultant sulfide in the hydrodesulfurization (HDS) of COS. Co_3O_4 nanorods are enclosed by four {110} and two {001} planes, while the nanopolyhedra are enclosed by eight {111} and six {100} planes. The exposure of the {110} surface, wherein Co^{3+} cations were present solely on, might lead to stronger reactivity of the nanorods than that of the nanopolyhedra, and promote the formation of more sulfur species on the rods during the presulfurization stage, then increasing the HDS activity for COS.[95]

Similarly, γ-Fe_2O_3 nanorods dominantly bound with {110} and {001} planes showed superior catalytic activity towards the comproportionation reaction between NO and NH_3. The coexistence of iron and oxygen ions on the surface of the γ-Fe_2O_3 nanorods is the key point. α-Fe_2O_3 nanorod exposed {210} and {001} planes were tested as much less active, which was due to the fact that these Fe-terminated surfaces only provided ferric sites for the adsorption of NO and NH_3 without neighboring oxygen anions for their activation.[39] NO and NH_3 adsorbed on the ferric site and its neighboring basic oxygen site, and subsequently generated nitrogen and water, probably through surface nitrate pathways.[96] Tunnelled α-MnO_2 had a much higher NH_3-SCR activity than layered δ-MnO_2 under the same reaction conditions, with little influence of the surface area. On the (110) plane of α-MnO_2, there were many coordinatively unsaturated Mn cations, while on the (001) plane of δ-MnO_2, all Mn cations were coordinatively saturated. So, α-MnO_2 possessed more Lewis acid sites, on which ammonia was well adsorbed. Furthermore, α-MnO_2 had weaker Mn–O bonds and tunnel structures, which were beneficial for NH_3 adsorption.[97]

Moreover, the product selectivity in specific reactions is highly correlated with the crystal face exposed. For example, Capdevila-Cortada and López's group found that the regular (100) termination of CeO_2 was the only facet that allowed hydrogen evolution *via* a hydride-hydroxyl precursor through density functional theory (DFT) calculations in the methanol decomposition reaction. Hydrogen evolution was allowed on the (100) facet, rather than on close-packed (111) and (110) facets. The formation of H–H bonds was due to the inherent defective sites in the former, that stabilizes two hydrogen atoms as hydroxyls and hydrides. (111) and (110) surfaces after the reduction could present enough vacancy sites to allow for similar chemistry on the close-packed facets. These active sites extended the lifetime of adsorbed HCHO, and then enabled its decomposition. In this case, the active sites were ultimately responsible for CO formation. Therefore, CeO_2 with different facets underwent different processes in methanol decomposition.[40]

3.2 Shape-controlled mixed valent oxides as catalyst supports

The oxygen vacancies of mixed valent oxides promote the activity of oxidation reactions. When mixed valent oxides serve as supports in catalysis, they can enhance the activity of active sites by several different routes. The reactivity of mixed valent oxide supported catalysts is always higher than normal oxide supported ones.[98] The facets of mixed valent oxides have an influence on the activity of shape-dependent catalysis.

There was such shape-dependent catalytic properties in the water gas shift (WGS) reaction, when those CeO_2 NCs served as supports.[37] The Flytzani-Stephanopoulos group presented the relationship between activity and crystal plane exposed ({111}, {100}, {110}) of nanoscale ceria as a support for gold in the WGS reaction. First, ceria nanorods ({110} and {100}), nanocubes ({100}), and nanopolyhedra ({111} and {100})[35] were synthesized using a hydrothermal method. Then gold was loaded by a deposition/precipitation (DP) method. The "light-off" WGS reaction profiles in Fig. 9 illustrate that the activity of the three Au/CeO_2 catalysts can be ranked as: rod > polyhedron > cube. The CO conversion over the rod sample was close to 100% (approx. 90%) at 250 °C, while the cube sample achieved only around 20% at 350 °C. Theoretical calculations showed that the formation energy of anion vacancies followed the order of {110} < {100} < {111} for CeO_2,[99] which meant that oxygen vacancies were easier to form on the CeO_2 {110} planes. Therefore, ceria nanorods should be better supports for anchoring and dispersing very fine gold clusters. These results explain the higher reducibility and activity of CeO_2 nanorod supported Au catalysts in the WGS reaction and the more significant dispersion and stability of gold on CeO_2 nanorods.[37]

In the oxidation of trace ethylene, mesoporous Co_3O_4 with {110} planes was more active, compared with Co_3O_4 nanosheets enclosed by {112} planes. It was found that Co_3O_4 with {110} planes exhibited high ethylene oxidation activity at 0 °C, while no activity was observed over Co_3O_4 nanosheets. The {110} planes, which Co^{3+} cations were present solely on, were regarded as the active sites for ethylene oxidation, and then sufficient Co^{3+} cations on the {110} planes would provide

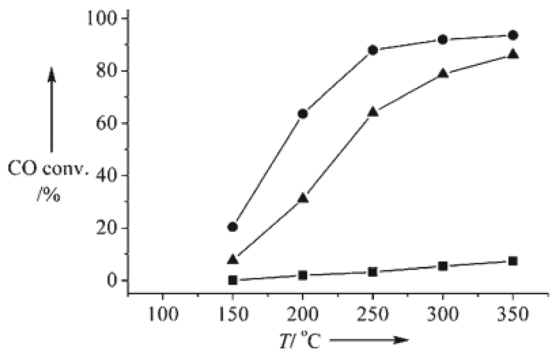

Fig. 9 WGS reaction "light-off" profiles for 1% Au on CeO_2 nanorods (●), cubes (■), and polyhedra (▲) (modified with permission from ref. 37, copyright 2008 Wiley-VCH).

abundant sites for ethylene. It was inferred that the {110} planes were the mainly active planes for ethylene oxidation. The mesoporous Au/Co_3O_4 catalyst had well-dispersed Au nanoparticles on the porous Co_3O_4 matrix, which provided a great number of active gold sites and led to high activity in ethylene oxidation (76% conversion at 0 °C).[100] Through further study, Au/Co_3O_4 catalysts with different morphologies (nanorods, nanopolyhedra and nanocubes) were formed and evaluated for complete ethylene oxidation. Compared with {011} and {001} planes, the {110} planes had the maximum amount of oxygen vacancies, which played a major role in ethylene oxidation.[101]

3.3 Shape-controlled mixed valent oxides as photocatalysts

As mentioned in the previous sections, most mixed valent oxides are semiconductors. Those oxides, especially TiO_2, have been applied in photocatalysis and photovoltaic devices. Because of quantum confined effects and the high surface area brought about by nanoscale effects, semiconductor NCs have gained broad multidisciplinary interest. As photocatalysts, oxide NCs can degrade organic waste under ultraviolet radiation on one hand. On the other hand, they can adsorb solar energy and split water into hydrogen and oxygen with the purpose of generating clean energy. The efficiency of photocatalysis is dependent on the bandgap and recombination of photon-generated carriers. Also the chemical activity of exposed facets contributes to photocatalysis processes. The bandgap can be modulated by the size of NCs and the doped ions. With different exposed facets, the chemical activity of NCs changes. And the recombination of photon-generated carriers is influenced by many factors (*e.g.*, size, exposed facets, conjunction with metals, *etc.*). Similar to heterogeneous catalysis, the photocatalytic properties of mixed valent oxides are structure-sensitive.[44,45,71,102–104]

Constructing high energy planes is a valid way to enhance photocatalytic activity. Compared with other basic planes, {001} is the high energy surface in anatase TiO_2 NCs. Much research work has been undertaken for fabricating anatase nanostructures with a high percentage of {001} planes.[44–46] These nanostructures show high photocatalytic activity in the degradation of organic waste. The photocatalytic activity of anatase TiO_2 NCs in both photoreduction and photooxidation processes could be enhanced by strengthened spontaneously surface-induced separation between photogenerated electrons and holes in the photocatalysis process.[102] Recent work on building atomic-scale nanostructures and high index facets could be considered as the extreme examples of the fabrication of high energy planes.[103]

There are also several similar cases of the synthesis of nanocatalysts with exposed high energy surface in Cu_2O systems.[78,80] Rhombic dodecahedra revealed that only the {110} facets exhibited an exceptionally good photocatalytic activity, which was shown in the fast and complete photodegradation of methyl orange, due to the more positively charged {110} facets compared to the {111} and {100} facets, due to the high number density of {110} surface copper atoms.[71]

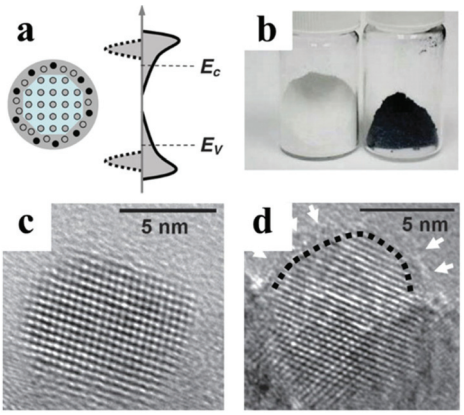

Fig. 10 (a) Scheme of the structure and band gap of TiO_2 black; (b) photographs of TiO_2 white (left) and TiO_2 black (right) samples; High Resolution Transmission Electron Microscopy (HRTEM) images of (c) anatase NCs and (d) TiO_2 black (modified with permission from ref. 104, copyright 2011 American Association for the Advancement of Science).

For ZnO nanostructures, the optical properties can be influenced by the number of oxygen defects, which can be generated by a large fraction of polar planes.[105,106] Oxygen vacancies are likely generated on polar planes, therefore they are expected to prevent electron–hole recombination, resulting in increased photocatalytic activity.[107] Using the photocatalytic degradation of methylene blue as a model system, morphology-dependent enhanced photoactivity under UV-light could be studied, and the order of the photocatalytic efficiency was consistent with the surface area and the percentage of exposed polar facets of ZnO nanostructures.[108]

Besides these well-known strategies for the adjustment of photocatalytic efficiency, Mao's group has introduced disorder into TiO_2 NCs (Fig. 10).[104] In some industry catalytic processes, efficient amorphous catalysts (*e.g.*, alloys *etc.*) have already been used for several decades. Here, the lattice-disordered "TiO_2 black" exhibited higher efficiency than anatase nanostructures. The lattice disorder not only induced a mid-gap state to improve the visible and infrared optical absorption, but also delayed the recombination of photon-generated carriers. This "disorder engineering" strategy can be also used for other metal oxides. Until now, the fabrication of highly efficient photocatalysts remains a challenge. The progress made in synthetic methods and theoretical calculations is expected to promote the enhancement of the efficiency of such photocatalysts.

Conclusions

Generally, in order to obtain enhanced catalytic activity and selectivity, the aim of shape-controlled synthesis is to synthesize nano- or microcrystallites with high surface energy facets. The regulation of thermodynamics and dynamics of the synthetic process is the foundation of all synthetic routes. As

Scheme 1 illustrates, tuning the surface atom arrangement and the associated active sites of oxide NCs can be achieved through several universal shape control strategies: selective adsorption of specific crystal facets, intermediate transformation, addition of mineralizers and templating surfactants, adjusting the pH value of the reaction medium, selective etching, galvanic replacement and the Kirkendall effect.

The selective adsorption approach will be instructive in the cognition of surface property and the selection of structure sensitive reactions by strong affinity to certain crystalline planes and stabilizing them by reducing the surface energy. Through the addition of these adsorption species, NCs with identical crystalline plane can be acquired. Size and morphology can be tuned by varying the species and concentration of surfactant. Surfactants not only prevent small particles from aggregation, but also reduce the surface energy of nanoparticles. Surface energy is the key point in determining the final morphology in most cases. Also the adoption of surfactant is beneficial to the self-assembly behavior of NCs and organic–inorganic complexes as a soft template, which provides a valid way to fabricate NCs with different shapes. However, the surfactant which is used in the controllable synthesis will hinder the surface sites to interact with other molecules and severely reduce the catalytic activity of the catalysts. Therefore, it is necessary to establish efficient non-destructive methods to remove surfactant or explore surfactant-free synthetic approaches for achieving much enhanced catalytic performance. The regulation of acid–base balance is widely applied in these methods. The regulation of acid–base can adjust the shapes, sizes, and crystal phases of mixed valent oxide NCs as a result of the interplay between thermodynamics and kinetics. The acid–base balance can affect the dissolution/recrystallization process and growth rate of metal oxides NCs.[71] It can regulate the surface charge and surface potential of mixed valent oxide, and can also control the shape of intermediates. The crystalline phase of nuclei or intermediates is critical for shape controlled synthesis. Formation of 1D or 2D structured cubic oxides mainly results from the anisotropic growth of the intermediate. Furthermore, some complex structures are fabricated by selective etching, galvanic replacement, or the Kirkendall effect.

Although plentiful synthetic methods of well-shaped mixed valent oxide NCs have been reported, only some of the NCs were studied for their shape-dependent catalytic properties. Nevertheless due to the similar structural features in mixed valent oxides, the conclusions of structure activity relationships drawn from thoroughly-studied systems should be applied to other oxides. Sizes, crystal planes, and oxygen vacancies (*i.e.*, defects) play key roles in tuning the catalytic properties of mixed valent oxide NCs. Highly unsaturated atoms on the surface are regarded as the active sites given their strong affinity to other molecules. These kinds of sites exists on defects, high-index facets, edges and clusters. Hence, it is a feasible strategy to design highly efficient catalysts by the synthesis of defective NCs at an atomic level or high-index-facet-exposed NCs with novel structures (*e.g.*, hollow structure, ultrathin 1D or 2D structure, *etc.*). Also attributed to the increase of oxygen vacancies or dipole–dipole interaction, catalytic activity may be improved by the doping of foreign ions.[3–6]

In the view of catalysis, most catalytic reactions are carried out under reductive or oxidative atmosphere. So the "active phase" of mixed valent oxide nanocatalysts is probably not itself but the redox product. The phase, sometimes even the size and morphology may change during the catalytic reaction. Operando characterization is able to uncover the factors governing the molecular catalytic mechanism (*e.g.*, the crystalline phase, defect sites, adsorption behaviours of reactants, metal–support interaction, *etc.*) during the reaction.[109–112] This will be also beneficial for the understanding of the catalysis process and the further design of robust catalysts.

First-principles based theoretical calculations have become a more and more powerful method to interpret the molecular catalytic mechanism from microscopic energy and guide the design of catalysts with high performance.[113] It is also helpful to clarify the possible synthetic mechanism. More and more rationally designed work is being carried out based on the conduct of theoretical calculations.

To sum up, in this review, we summarize the research works on the controllable synthesis of mixed valent oxide NCs and their structure-dependent catalytic properties. Well-shaped NCs provide a good model for the investigation of the relevance between catalytic properties and structural features. With the suggested catalysis mechanism as feedback, highly efficient nanocatalysts are able to be achieved through rationally designed synthetic routes. The scheme on rational design and fabrication of high performance nanocatalysts with manipulated shapes of mixed valent oxides will be an attractive model for future research into nanocatalysis with broad interest and applications.

Acknowledgements

This work was supported by the National Science Foundation of China (NSFC) (Grant No. 21025101, 21271011, 21573005, and 21321001). Y.W.Z. particularly appreciates the financial aid of China National Funds for Distinguished Young Scientists from the NSFC.

Notes and references

1 D. A. Andersson, S. I. Simak, N. V. Skorodumova, I. A. Abrikosov and B. Johansson, *Proc. Natl. Acad. Sci. U. S. A.*, 2006, **103**, 3518.
2 C. T. Campbell and C. H. F. Peden, *Science*, 2005, **309**, 713.
3 S. Royer and D. Duprez, *ChemCatChem*, 2011, **3**, 24.
4 R. Si, Y. W. Zhang, S. J. Li, B. X. Lin and C. H. Yan, *J. Phys. Chem. B*, 2004, **108**, 12481.
5 R. Si, Y. W. Zhang, L. M. Wang, S. J. Li, B. X. Lin, W. S. Chu, Z. Y. Wu and C. H. Yan, *J. Phys. Chem. B*, 2007, **111**, 787.

6 S. R. Bishop, K. L. Duncan and E. D. Wachsman, *Acta Mater.*, 2009, **57**, 3596.
7 R. V. D. Krol, Y. Q. Liang and J. Schoonman, *J. Mater. Chem.*, 2008, **18**, 2311.
8 A. Fujishima and K. Honda, *Nature*, 1972, **238**, 37.
9 B. Oregan and M. Gratzel, *Nature*, 1991, **353**, 737.
10 K. L. Kobayashi, T. Kimura, H. Sawada, K. Terakura and Y. Tokura, *Nature*, 1998, **395**, 677.
11 C. W. Nan, M. I. Bichurin, S. X. Dong, D. Viehland and G. Srinivasan, *J. Appl. Phys.*, 2008, **103**, 031101.
12 C. Hagleitner, A. Hierlemann, D. Lange, A. Kummer, N. Kerness, O. Brand and H. Baltes, *Nature*, 2001, **414**, 293.
13 A. K. Gupta and M. Gupta, *Biomater.*, 2005, **26**, 3995.
14 P. T. Anastas and M. M. Kirchhoff, *Acc. Chem. Res.*, 2002, **35**, 686.
15 M. Shelef and R. W. McCabe, *Catal. Today*, 2000, **62**, 35.
16 E. Iglesia, S. C. Reyes and R. J. Madon, *J. Catal.*, 1991, **129**, 238.
17 B. C. H. Steele and A. Heinzel, *Nature*, 2001, **414**, 345.
18 A. Fritz and V. Pitchon, *Appl. Catal., B*, 1997, **13**, 1.
19 M. Guisnet and P. Magnoux, *Appl. Catal., A*, 2001, **212**, 83.
20 Q. Fu, H. Saltsburg and M. Flytzani-Stephanopoulos, *Science*, 2003, **301**, 935.
21 Q. Fu, W. X. Li, Y. X. Yao, H. Y. Liu, H. Y. Su, D. Ma, X. K. Gu, L. M. Chen, Z. Wang, H. Zhang, B. Wang and X. H. Bao, *Science*, 2010, **328**, 1141.
22 X. W. Xie, Y. Li, Z. Q. Liu, M. Haruta and W. J. Shen, *Nature*, 2009, **458**, 746.
23 I. X. Green, W. J. Tang, M. Neurock and J. T. Yates, *Science*, 2011, **333**, 736.
24 R. V. D. Krol, Y. Q. Liang and J. Schoonman, *J. Mater. Chem.*, 2008, **18**, 2311.
25 W. X. Huang and Y. X. Gao, *Catal. Sci. Technol.*, 2014, **4**, 3772.
26 Y. Li and W. J. Shen, *Chem. Soc. Rev.*, 2014, **43**, 1543.
27 J. J. Shan, Y. Zhu, S. R. Zhang, T. Zhu, S. Rouvimov and F. Tao, *J. Phys. Chem. C*, 2013, **117**, 8329.
28 Y. W. Jun, J. S. Choi and J. Cheon, *Angew. Chem., Int. Ed.*, 2006, **45**, 3414.
29 S. G. Kwon and T. Hyeon, *Acc. Chem. Res.*, 2008, **41**, 1696.
30 T. D. Nguyen and T. O. Do, Size- and Shape-Controlled Synthesis of Monodisperse Metal Oxide and Mixed Oxide Nanocrystals, in *Nanocrystal*, ed. Y. Masuda, 2011.
31 Q. Kuang, X. Wang, Z. Y. Jiang, Z. X. Xie and L. S. Zheng, *Acc. Chem. Res.*, 2014, **47**, 308.
32 M. Hua, S. J. Zhang, B. C. Pan, W. M. Zhang, L. Lv and Q. X. Zhang, *J. Hazard. Mater.*, 2012, **211–212**, 317.
33 M. Sarikaya, C. Tamerler, A. K. Y. Jen, K. Schulten and F. Baneyx, *Nat. Mater.*, 2003, **2**, 577.
34 A. Kolmakov and M. Moskovits, *Annu. Rev. Mater. Res.*, 2004, **34**, 151.
35 H. X. Mai, L. D. Sun, Y. W. Zhang, R. Si, W. Feng, H. P. Zhang, H. C. Liu and C. H. Yan, *J. Phys. Chem. B*, 2005, **109**, 24380.
36 N. J. Lawrence, J. R. Brewer, L. Wang, T. S. Wu, J. Wells–Kingsbury, M. M. Ihrig, G. H. Wang, Y. L. Soo, W. N. Mei and C. L. Cheung, *Nano Lett.*, 2011, **11**, 2666.
37 R. Si and M. Flytzani-Stephanopoulos, *Angew. Chem., Int. Ed.*, 2008, **47**, 2884.
38 M. Leng, M. Z. Liu, Y. B. Zhang, Z. Q. Wang, C. Yu, X. G. Yang, H. J. Zhang and C. Wang, *J. Am. Chem. Soc.*, 2010, **132**, 17084.
39 X. L. Mou, B. S. Zhang, Y. Li, L. D. Yao, X. J. Wei, D. S. Su and W. J. Shen, *Angew. Chem., Int. Ed.*, 2012, **51**, 2989.
40 M. C. Cortada, M. G. Melchor and N. López, *J. Catal.*, 2015, **327**, 58.
41 L. D. Marks, *Rep. Prog. Phys.*, 1994, **57**, 603.
42 T. R. Gordon, M. Cargnello, T. Paik, F. Mangolini, R. T. Weber, P. Fornasiero and C. B. Murray, *J. Am. Chem. Soc.*, 2012, **134**, 6751.
43 X. M. Yu, B. Jeon and Y. K. Kim, *ACS Catal.*, 2015, **5**, 3316.
44 H. G. Yang, C. H. Sun, S. Z. Qiao, J. Zou, G. Liu, S. C. Smith, H. M. Cheng and G. Q. Lu, *Nature*, 2008, **453**, 638.
45 X. G. Han, Q. Kuang, M. S. Jin, Z. X. Xie and L. S. Zheng, *J. Am. Chem. Soc.*, 2009, **131**, 3152.
46 X. H. Yang, Z. Li, C. H. Sun, H. G. Yang and C. Z. Li, *Chem. Mater.*, 2011, **23**, 3486.
47 D. Zitoun, N. Pinna, N. Frolet and C. Belin, *J. Am. Chem. Soc.*, 2005, **127**, 15034.
48 C. J. Jia, L. D. Sun, Z. G. Yan, L. P. You, F. Luo, X. D. Han, Y. C. Pang, Z. Zhang and C. H. Yan, *Angew. Chem., Int. Ed.*, 2005, **44**, 4328.
49 X. L. Hu, J. C. Yu, J. M. Gong, Q. Li and G. S. Li, *Adv. Mater.*, 2007, **19**, 2324.
50 Z. C. Xu, C. M. Shen, Y. A. Tian, X. Z. Shi and H. J. Gao, *Nanoscale*, 2010, **2**, 1027.
51 B. L. Lv, Z. Y. Liu, H. Tian, Y. Xu, D. Wu and Y. H. Sun, *Adv. Funct. Mater.*, 2010, **20**, 3987.
52 K. X. Yao, X. M. Yin, T. H. Wang and H. C. Zeng, *J. Am. Chem. Soc.*, 2010, **132**, 6131.
53 D. F. Zhang, H. Zhang, L. Guo, K. Zheng, X. D. Han and Z. Zhang, *J. Mater. Chem.*, 2009, **19**, 5220.
54 Y. M. Sui, W. Y. Fu, H. B. Yang, Y. Zeng, Y. Y. Zhang, Q. Zhao, Y. E. Li, X. M. Zhou, Y. Leng, M. H. Li and G. T. Zou, *Cryst. Growth Des.*, 2010, **10**, 99.
55 Y. W. Tan, X. Y. Xue, Q. Peng, H. Zhao, T. H. Wang and Y. D. Li, *Nano Lett.*, 2007, **7**, 3723.
56 M. J. Siegfried and K. S. Choi, *J. Am. Chem. Soc.*, 2006, **128**, 10356.
57 S. Hu and X. Wang, *J. Am. Chem. Soc.*, 2008, **130**, 8126.
58 S. W. Yang and L. Gao, *J. Am. Chem. Soc.*, 2006, **128**, 9330.
59 J. Zhang, S. Ohara, M. Umetsu, T. Naka, Y. Hatakeyama and T. Adschiri, *Adv. Mater.*, 2007, **19**, 203.
60 C. C. Tang, Y. Bando, B. D. Liu and D. Golberg, *Adv. Mater.*, 2005, **17**, 3005.
61 L. H. Hu, Q. Peng and Y. D. Li, *J. Am. Chem. Soc.*, 2008, **130**, 16136.
62 R. Inguanta, S. Piazza and C. Sunseri, *Nanotechnol.*, 2007, **18**, 485605.

63 K. B. Zhou, X. Wang, X. M. Sun, Q. Peng and Y. D. Li, *J. Catal.*, 2005, **229**, 206.
64 D. Y. Wang, Y. J. Kang, V. D. Nguyen, J. Chen, R. Küngas, N. L. Wieder, K. Bakhmutsky, R. J. Gorte and C. B. Murray, *Angew. Chem., Int. Ed.*, 2011, **50**, 4378.
65 Y. L. Zhang, J. Zhu, X. Song and X. H. Zhong, *J. Phys. Chem. C*, 2008, **112**, 5322.
66 Y. P. Du, Y. W. Zhang, L. D. Sun and C. H. Yan, *J. Phys. Chem. C*, 2009, **113**, 6521.
67 Z. Y. Huo, C. K. Tsung, W. Y. Huang, M. Fardy, R. X. Yan, X. F. Zhang, Y. D. Li and P. D. Yang, *Nano Lett.*, 2009, **9**, 1260.
68 C. K. Tsung, J. Fan, N. F. Zheng, Q. H. Shi, A. J. Forman, J. F. Wang and G. D. Stucky, *Angew. Chem., Int. Ed.*, 2008, **47**, 8682.
69 T. Yu, B. Lim and Y. N. Xia, *Angew. Chem., Int. Ed.*, 2010, **49**, 4484.
70 J. Park, E. Kang, C. J. Bae, J. G. Park, H. J. Noh, J. Y. Kim, J. H. Park, H. M. Park and T. Hyeon, *J. Phys. Chem. B*, 2004, **108**, 13594.
71 W. C. Huang, L. M. Lyu, Y. C. Yang and M. H. Huang, *J. Am. Chem. Soc.*, 2012, **134**, 1261.
72 S. I. Cha, K. H. Hwang, Y. H. Kim, M. J. Yun, S. H. Seo, Y. J. Shin, J. H. Moon and D. Y. Lee, *Nanoscale*, 2013, **5**, 753.
73 D. Portehault, S. Cassaignon, E. Baudrin and J. P. Jolivet, *J. Mater. Chem.*, 2009, **19**, 7947.
74 Z. H. Zhao, J. Tian, Y. H. Sang, A. Cabot and H. Liu, *Adv. Mater.*, 2015, **27**, 2557.
75 N. Q. Wu, J. Wang, D. Tafen, H. Wang, J. G. Zheng, J. P. Lewis, X. G. Liu, S. S. Leonard and A. Manivannan, *J. Am. Chem. Soc.*, 2010, **132**, 6679.
76 F. Pan, K. Wu, H. X. Li, G. Q. Xu and W. Chen, *Chem. – Eur. J.*, 2014, **20**, 15095.
77 B. Zhao, L. Lin, C. Chen, Y. C. Chai and D. N. He, *Acta Chim. Sin.*, 2013, **71**, 93.
78 S. D. Sun, D. C. Deng, C. C. Kong, Y. Gao, S. C. Yang, X. P. Song, B. J. Ding and Z. M. Yang, *CrystEngComm*, 2011, **13**, 5993.
79 Z. Y. Wang, D. Y. Luan, C. M. Li, F. Su, S. Madhavi, F. Y. C. Boey and X. W. Lou, *J. Am. Chem. Soc.*, 2010, **132**, 16271.
80 C. H. Kuo and M. H. Huang, *J. Am. Chem. Soc.*, 2008, **130**, 12815.
81 B. D. Anderson and J. B. Tracy, *Nanoscale*, 2014, **6**, 12195.
82 M. H. Oh, T. Yu, S. H. Yu, B. Lim, K. T. Ko, M. G. Willinger, D. H. Seo, B. H. Kim, M. G. Cho, J. H. Park, K. Kang, Y. E. Sung, N. Pinna and T. Hyeon, *Science*, 2013, **340**, 964.
83 W. Yao, F. L. Li, H. X. Li and J. P. Lang, *J. Mater. Chem. A*, 2015, **3**, 4578.
84 S. Peng and S. H. Sun, *Angew. Chem., Int. Ed.*, 2007, **46**, 4155.
85 Z. J. Yang, M. Walls, I. Lisiecki and M. P. Pileni, *Chem. Mater.*, 2013, **25**, 2372.
86 Z. J. Yang, I. Lisiecki, M. Walls and M. P. Pileni, *ACS Nano*, 2013, **7**, 1342.
87 J. Ke, W. Zhu, Y. Y. Jiang, R. Si, Y. J. Wang, S. C. Li, C. H. Jin, H. C. Liu, W. G. Song, C. H. Yan and Y. W. Zhang, *ACS Catal.*, 2015, **5**, 5164.
88 F. Esch, S. Fabris, L. Zhou, T. Montini, C. Africh, P. Fornasiero, G. Comelli and R. Rosei, *Science*, 2005, **309**, 752.
89 T. X. T. Sayle, S. C. Parker and C. R. A. Catlow, *Surf. Sci.*, 1994, **316**, 329.
90 J. C. Conesa, *Surf. Sci.*, 1995, **339**, 337.
91 J. J. Ouyang, J. Pei, Q. Kuang, Z. X. Xie and L. S. Zheng, *ACS Appl. Mater. Interfaces*, 2014, **6**, 12505.
92 X. W. Liu, K. B. Zhou, L. Wang, B. Y. Wang and Y. D. Li, *J. Am. Chem. Soc.*, 2009, **131**, 3140.
93 J. Ke, J. W. Xiao, W. Zhu, H. C. Liu, R. Si, Y. W. Zhang and C. H. Yan, *J. Am. Chem. Soc.*, 2013, **135**, 15191.
94 Y. J. Wang, H. Dong, G. M. Lyu, H. Y. Zhang, J. Ke, L. Q. Kang, J. L. Teng, L. D. Sun, R. Si, J. Zhang, Y. J. Liu, Y. W. Zhang, Y. H. Huang and C. H. Yan, *Nanoscale*, 2015, **7**, 13981.
95 X. Wang, L. Ding, Z. Zhao, W. Xu, B. Meng and J. Qiu, *Catal. Today*, 2011, **175**, 509.
96 A. Grossale, I. Nova, E. Tronconi, D. Chatterjee and M. Weibel, *J. Catal.*, 2008, **256**, 312.
97 D. Yun, L. J. Hua, P. Yue and T. X. Fu, *Acta Phys. Chim. Sin.*, 2012, **28**, 1771.
98 B. Zhang, S. Kaziz, H. Li, M. G. Hevia, D. Wodka, C. Mazet, T. Bürgi and N. Barrabés, *J. Phys. Chem. C*, 2015, **119**, 11193.
99 T. X. T. Sayle, S. C. Parker and D. C. Sayle, *Phys. Chem. Chem. Phys.*, 2005, **7**, 2936.
100 C. Y. Ma, Z. Mu, J. J. Li, Y. G. Jin, J. Cheng, G. Q. Lu, Z. P. Hao and S. Z. Qiao, *J. Am. Chem. Soc.*, 2010, **132**, 2608.
101 W. J. Xue, Y. F. Wang, P. Li, Z. T. Liu, Z. P. Hao and C. Y. Ma, *Catal. Commun.*, 2011, **12**, 1265.
102 C. Liu, X. G. Han, S. F. Xie, Q. Kuang, X. Wang, M. S. Jin, Z. X. Xie and L. S. Zheng, *Chem. – Asian J.*, 2013, **8**, 282.
103 C. M. Liu and S. H. Yang, *ACS Nano.*, 2009, **3**, 1025.
104 X. B. Chen, L. Liu, P. Y. Yu and S. S. Mao, *Science*, 2011, **331**, 746.
105 S. He, S. T. Zhang, J. Lu, Y. F. Zhao, J. Ma, M. Wei, D. G. Evans and X. Duan, *Chem. Commun.*, 2011, **47**, 10797.
106 V. Ischenko, S. Polarz, D. Grote, V. Stavarache, K. Fink and M. Driess, *Adv. Funct. Mater.*, 2005, **15**, 1945.
107 G. R. Li, T. Hu, G. L. Pan, T. Y. Yan, X. P. Gao and H. Y. Zhu, *J. Phys. Chem. C*, 2008, **112**, 11859.
108 R. Boppella, K. Anjaneyulu, P. Basak and S. V. Manorama, *J. Phys. Chem. C*, 2013, **117**, 4597.
109 C. Rameshan, W. Stadlmayr, S. Penner, H. Lorenz, N. Memmel, M. Havecker, R. Blume, D. Teschner, T. Rocha, D. Zemlyanov, A. Knop-Gericke, R. Schlogl and B. Klotzer, *Angew. Chem., Int. Ed.*, 2012, **51**, 3002.
110 E. de Smit, I. Swart, J. F. Creemer, G. H. Hoveling, M. K. Gilles, T. Tyliszczak, P. J. Kooyman, H. W. Zandbergen,

C. Morin, B. M. Weckhuysen and F. M. F. de Groot, *Nature*, 2008, **456**, 222.
111 F. Tao, S. Dag, L. W. Wang, Z. Liu, D. R. Butcher, H. Bluhm, M. Salmeron and G. A. Somorjai, *Science*, 2010, **327**, 850.
112 H. Yoshida, Y. Kuwauchi, J. R. Jinschek, K. J. Sun, S. Tanaka, M. Kohyama, S. Shimada, M. Haruta and S. Takeda, *Science*, 2012, **335**, 317.
113 A. U. Nilekar, S. Alayoglu, B. Eichhorn and M. Mavrikakis, *J. Am. Chem. Soc.*, 2010, **132**, 7418.